



Contents lists available at ScienceDirect

Journal of Biomechanics

journal homepage: www.elsevier.com/locate/jbiomech
www.JBiomech.com

Scanner influence on the mechanical response of QCT-based finite element analysis of long bones

Yekutiel Katz^{a,1}, Gal Dahan^{a,1}, Jacob Sosna^b, Ilan Shelef^c, Evgenia Cherniavsky^d, Zohar Yosibash^{a,*}^a School of Mechanical Engineering, Tel Aviv University, Ramat Aviv, Israel^b Department of Radiology & Medical Imaging, Hadassah Hebrew University Medical Center, Jerusalem, Israel^c Diagnostic Imaging Institute, Soroka University Medical Center, Beer Sheva, Israel^d Department of Radiology, Barzilai Medical Center, Ashkelon, Israel

ARTICLE INFO

Article history:

Accepted 30 January 2019

Keywords:

QCT
Femur
Finite element analysis
Humerus
Patient-specific
Personalized medicine

ABSTRACT

Patient-specific QCT-based finite element (QCTFE) analyses enable highly accurate quantification of bone strength. We evaluated CT scanner influence on QCTFE models of long bones.

A femur, humerus, and proximal femur without the head were scanned with K_2HPO_4 phantoms by seven CT scanners (four models) using typical clinical protocols. QCTFE models were constructed. The geometrical dimensions, as well as the QCT-values expressed in Hounsfield unit (HU) distribution was compared. Principal strains at representative regions of interest (ROIs), and maximum principal strains (associated with fracture risk) were compared. Intraclass correlation coefficients (ICCs) were calculated to evaluate strain prediction reliability for different scanners. Repeatability was examined by scanning the femur twice and comparing resulting QCTFE models.

Maximum difference in geometry was 2.3%. HU histograms before phantom calibration showed wide variation between QCT scans; however, bone density histogram variability was reduced after calibration and algorithmic manipulation. Relative standard deviation (RSD) in principal strains at ROIs was <10.7%. ICC estimates between scanners were >0.9. Fracture-associated strain had 6.7%, 8.1%, and 13.3% maximum RSD for the femur, humerus, and proximal femur, respectively. The difference in maximum strain location was <2 mm. The average difference with repeat scans was 2.7%.

Quantification of strain differences showed mean RSD bounded by ~6% in ROIs. Fracture-associated strains in “regular” bones showed a mean RSD bounded by ~8%. Strains were obtained within a ±10% difference relative to the mean; thus, in a longitudinal study only changes larger than 20% in the principal strains may be significant. ICCs indicated high reliability of QCTFE models derived from different scanners.

© 2019 Elsevier Ltd. All rights reserved.

1. Introduction

Personalized finite element (FE) models of bones based on quantitative computed tomography (QCT) have been used extensively to estimate bone stiffness and strength. Among these, the human femur and humerus attracted significant interest (Dahan et al., 2016; Dall'Ara et al., 2013; Enns-Bray et al., 2016; Hazrati Marangalou et al., 2012; Helgason et al., 2014; Keaveny et al., 2008; Keyak et al., 2005, 1990; Nishiyama et al., 2013; Pise et al., 2009; Schileo et al., 2008a; Trabelsi et al., 2011; Yosibash

et al., 2007b) because of their importance for fracture risk prediction due to osteoporosis, optimal management of bony metastases, and more. QCT-based FE (QCTFE) analysis is considered one of the best current techniques for noninvasive assessment of femoral and humeral strength (Keaveny et al., 2010).

Validation of QCTFE predictions has been performed by comparing predicted strain on bone surface and fracture load to these measured in ex vivo experiments (Dahan et al., 2016; Trabelsi et al., 2011; Yosibash et al., 2007b). Most validation studies were based on QCT scans performed on a single scanner; however, to introduce QCTFE into clinical practice for longitudinal studies in diverse clinical centers, scanner influence on QCTFE predictions must be quantified. QCTFE models are directly affected by QCT data: (a) bone geometry is reconstructed from the set of points sampled in the scan; (b) bone density in each voxel, a proxy for material properties, is derived from CT-values expressed in

* Corresponding author at: Computational Mechanics and Experimental Biomechanics Labs, School of Mechanical Engineering, POB 6139001, Tel Aviv, Israel.

E-mail address: yosibash@tauex.tau.ac.il (Z. Yosibash).

¹ Equal contribution.

Hounsfield unit (HU). Additionally, indirect effects are present due to algorithmic manipulations of QCT data: (a) boundary corrections and density averaging are performed at the voxel level to overcome the partial volume effect and to reduce noise; (b) material properties are determined using empirical relationships based on HUs and assigned to the FE model at specific locations (integration points).

The feasibility of introducing QCTFE into clinical use was recently addressed in a study examining QCTFE model dependence on scan protocols (Dragomir–Daescu et al., 2015). The paper concluded that predicted strength and stiffness of QCTFE models generated from ‘high’ and ‘low’ resolution scans could be different if CT settings and reconstruction techniques vary. A second study (Giambini et al., 2015) found that material property estimation may be dependent on scan parameters such as voltage and current as well as post-processing techniques, including the reconstruction kernel, with the differences potentially affecting estimates of strength and stiffness. The basic assumption that QCTFE models are independent of CT scanner was questioned based on a comparison of density and strength evaluated with two different scanners (Carpenter et al., 2014). The study concluded that significant inter-scanner differences remain even after using phantom calibration.

This study compares patient-specific QCTFE models using data obtained with multiple CT scanners and hospitals, while considering the steps in the QCTFE model construction pipeline. We analyzed scans of two human femurs and one humerus surrounded by five K_2HPO_4 phantoms. QCT scans were performed using standard clinical protocols. We hypothesized that a carefully designed and implemented pipeline would allow development of reliable QCTFE models of human bones, i.e. models that are virtually independent of the CT scanner used to acquire data.

2. Materials and methods

A femur from a 70-year-old female (51 kg, 170 cm), a humerus from a 57-year-old male (55 kg, 180 cm) (National Disease Research Institute, Philadelphia, PA), and a proximal femur without the head and neck from a 55-year-old male (73 kg, 175 cm) (ScienceCare Anatomical, Phoenix, AZ), were scanned by seven different CT scanners at four medical centers. In total, four CT scanner models from three manufacturers were used: Brilliance (64) and iCT (256) by Philips Healthcare (Eindhoven, The Netherlands), Somatom Definition Edge (128) by Siemens Medical Systems (Erlangen, Germany) and Optima CT660 (128) by GE HealthCare (Milwaukee, WI, USA).

Five liquid K_2HPO_4 phantoms (concentrations: 0, 50, 100, 200 and 300 mg/cc), prepared according to (Mindways Software, 2002) were used. The bones and phantoms were immersed in a water bath during all scans (Fig. 1A). Scans were performed according to a standard clinical protocol: exposure 210–500 mAs, X-ray tube voltage 120 kV, and slice thickness and spacing 1 mm in all protocols except for scan G, where it was 1.25 mm (see Table 2). Images were reconstructed using a “soft/body” filter/convolution kernel (B, B31f, and body filters for Philips, Siemens, and GE scanners, respectively). Details on CT scanners, medical centers and scanning protocols are presented in Tables 1 and 2.

2.1. Brief summary of QCTFE pipeline

FE models were generated using the various QCT scans according to a validated procedure (Yosibash et al., 2007a, 2007b). Strains, stiffness, and fracture loads computed by QCTFE models were previously validated in double-blind in vitro studies, where the modeling pipeline was described in detail (Trabelsi et al., 2011; Yosibash et al., 2014, 2010). Briefly, bone boundaries were

identified on each slice and surfaces were imported as a point cloud to a computer-aided design software program (SolidWorks by Dassault Systems, Waltham, MA, USA). All QCTFE models were aligned in a uniform coordinate system. This ensured that the same boundary conditions were applied and that results were extracted at the same locations in all models. Alignment was performed using an “iterative closest point” algorithm (CloudCompare, <http://www.danielgm.net/cc/>). Geometrical differences between models were due to differences in pixel size and the set of points from which each model was reconstructed. After alignment, these differences were assessed in 9–11 cross sections located along the bones at 12–25 mm intervals. Dimensions in x and y directions were extracted and the maximum differences at each section were compared to the average values.

HU calibration was performed by K_2HPO_4 phantoms: HU values were averaged along each phantom using a 10×10 mm² area at the center of 10 slices (3000–5800 pixels), see Fig. 1B. Five average HU values (five known densities in phantoms), determined a linear relationship between K_2HPO_4 density and HU: $\rho_{K_2HPO_4} = m \times HU + n$ (in all scans $R^2 > 0.998$). Values for m and n for each scan are given in last two columns of Table 2.

Due to the partial volume averaging effect in voxels on bone surface, a boundary correction algorithm was applied. A total width of ~ 1 mm, corresponding to 2 pixels, was usually affected. HU values in all voxels were corrected for noise effects by a moving average algorithm on a cubic volume of 27 bone voxels. Young’s modulus (pointwise “stiffness”) was thereafter computed based on ash density (ρ_{ash}), using the empirical relationship described in (Schileo et al., 2008a) and the relationship between hydroxyapatite and K_2HPO_4 densities (Goodsitt, 1992):

$$\rho_{ash} \left[\frac{g}{cc} \right] = 1.061 \times \rho_{K_2HPO_4} + 0.08 \quad (1)$$

CT scanner output data was compared by inspecting histograms of both raw HU and resulting ρ_{ash} obtained after moving average and boundary correction algorithms. An inhomogeneous Young’s modulus (E), based on ρ_{ash} for cortical (Keller, 1994) and trabecular bone (Keyak et al., 1994) was assigned to the QCTFE models, considering only values of $\rho_{ash} > 0$ $\left[\frac{g}{cc} \right]$:

$$E_{cort} = 10200 \times \rho_{ash}^{2.01} [\text{MPa}], \quad \rho_{ash} \geq 0.486 \left[\frac{g}{cc} \right] \quad (2)$$

$$E_{trab} = 2398 [\text{MPa}], \quad 0.3 < \rho_{ash} < 0.486 \left[\frac{g}{cc} \right] \quad (3)$$

$$E_{trab} = 33900 \times \rho_{ash}^{2.2} [\text{MPa}], \quad \rho_{ash} \leq 0.3 \left[\frac{g}{cc} \right] \quad (4)$$

The Poisson ratio was set to $\nu = 0.3$, as commonly used in bone QCTFE models (Schileo et al., 2014; Varga et al., 2018; Wirtz et al., 2000; Yosibash et al., 2007a).

On the femur head, a hip contact force representing a stance position of 1250N was applied parallel to the shaft axis on a 335 mm² area. On the humerus head, a $230N\hat{x} + 650N\hat{z}$ load was applied on a 320mm² area with the z axis rotated at 20° to the shaft axis and the x axis pointing laterally. On the proximal femur, a normal displacement $u_n = 0.75$ mm was applied on an area of 810 mm² inclined by 35° to the shaft axis (as illustrated in Fig. 2). All three bones were clamped at the distal surface ($\vec{u} = 0$). A mesh of p – tetrahedral elements with a maximum element volume of ~ 150 mm³ was generated. Linear elastic QCTFE analyses were performed by increasing the polynomial degree over elements from $p = 1$ to $p = 8$, to allow monitoring of numerical errors in energy norm and strains (Szabó and Babüska, 1991). We emphasize the advantages of p -FE methods (Trabelsi et al., 2011; Yosibash et al., 2007b) over conventional FE methods: they accurately represent

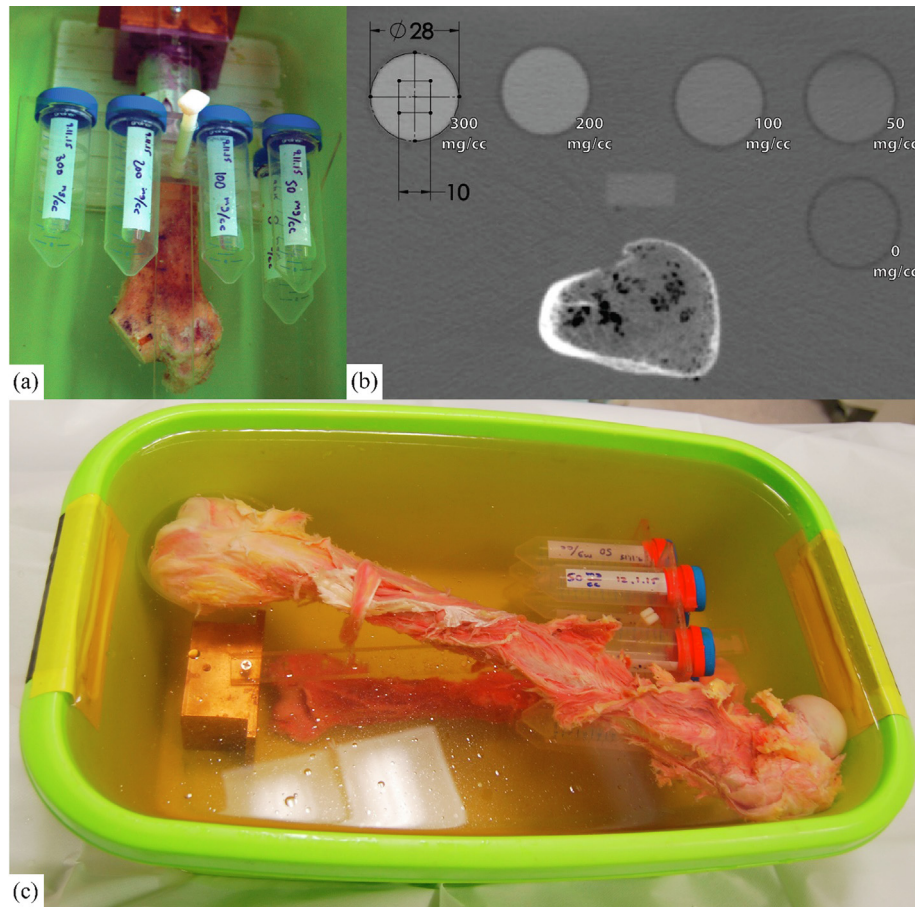


Fig. 1. (a) Proximal femur in the water bath surrounded by five liquid potassium phosphate (K_2HPO_4) phantoms. (b) A representative CT slice of the femur and phantoms. (c) Whole femur and humerus in water bath with the liquid phantoms.

Table 1
CT scanners and hospitals examined.

Scan abbreviation	Medical center	CT scanner model (# detector rows)
A	MC 1	Brilliance
B	MC 2	Philips Healthcare
C	MC 4	(64)
D	MC 1	iCT
E	MC 2	Philips Healthcare (256)
F	MC 3	Somatom Definition Edge Siemens Medical Systems (128)
G	MC 1	Optima CT660 GE HealthCare (128)

bone surfaces and polynomial degree (p) of shape functions is increased systematically to achieve convergence. p -FEs also allow a smooth variation of material properties within the model, elements are much larger, may be far more distorted, and produce considerably faster convergence rates.

To isolate the effect of the QCT reconstruction algorithm, we also performed FE analyses with a homogeneous Young's modulus, $E = 10$ GPa.

Comparison between QCTFE models was performed by means of principal strains (compression/tension), as they may serve as a criterion to predict femoral/humeral fracture (Bayraktar et al., 2004; Dahan et al., 2016; Schileo et al., 2014, 2008b; Yosibash

et al., 2010). Regions of interest (ROIs) on the bone surface were arbitrarily selected on the shaft, neck, and intertrochanteric/intertuberosity zones (13, 12, and 8 ROIs on the femur, humerus and proximal femur surfaces respectively, Fig. 2). ROIs were 3 mm lines resembling the commonly used strain gauges (SG) in validation experiments (Dahan et al., 2016; Katz et al., 2018; Yosibash et al., 2007b). The average strain value along each line was compared relatively to the mean strain value at a given ROI across all QCTFE models from the different scanners. Standard deviation of the strains was calculated for each ROI. Relative standard deviation (RSD [%], also known as coefficient of variation (CV)), defined by the ratio of the standard deviation to the mean strain in the ROI is reported. The mean RSD (averaged across all ROIs) for each bone is also presented. Based on the ROI strains, linear correlations were plotted for each pair of the QCTFE models.

To evaluate the reproducibility of results obtained from different scanners, intraclass correlation coefficient (ICC) estimates (two-way random effects, absolute agreement, single rater (Koo and Li, 2016; McGraw and Wong, 1996)) and their 95% confidence intervals (CI) were calculated using SPSS (IBM, Chicago, IL, USA). ICCs were calculated based on strain values in the different ROIs.

In addition to ROIs, indicating a global agreement between QCTFE models, the maximum tension and compression principal strains and their locations (surrogate of load to fracture and fracture location) were compared (averaged over a circular surface with a radius of $r = 2$ mm). To quantify and compare the obtained locations, a reference point representing the 'average' location was computed using least-mean-squares. We report mean, maximum, and RSD of the distance from the reference point.

Table 2
Detailed information on the different QCT scans. All scans performed at 120 kV.

Scan	Scanner (detector rows)	Date of scanning ^a	Exposure [mAs] [†]	Slice spacing & thickness (mm) ^{**}	Pixel size [mm]	$\rho_{K,HRQ} = m \times HU + n$	
						m	n
A	Philips Brilliance (64)	May 17, 2015 Jan 18, 2017	374 83–283	1	0.496 0.601	0.816 0.814	1.82 –3.20
B	Philips Brilliance (64)	Dec 12, 2015	232	1	0.46	0.795	3.08
C	Philips Brilliance (64)	Jan 18, 2017 July 19, 2016	223–370 301	1	0.523 0.492	0.818 0.793	–3.82 3.85
D	Philips iCT (256)	Jan 18, 2017 May 17, 2015	164 374	1	0.518 0.473	0.826 0.794	–4.50 0.60
E	Philips iCT (256)	Jan 18, 2017 Dec 12, 2015	81–106 406	1	0.557 0.574	0.811 0.806	–2.28 –2.96
F	Siemens Somatom Definition (128)	Jan 18, 2017 July 21, 2015	321–1104 210	1	0.502 0.440	0.813 0.869	–3.49 0.00
G	GE Optima CT660 (128)	Jan 18, 2017 May 17, 2015	96–215 500	1 1.25	0.621 0.523	0.857 0.823	0.89 1.00
		Jan 18, 2017	3–6	1.25	0.594	0.831	–6.83

[†] A range of mAs values indicates scans with adaptive current algorithm.

^{**} The slice thickness and slice spacing are equal for each scan.

^a Proximal femur was scanned during 2015, the regular bones during 2017.

Within-scanner repeatability of the QCTFE was examined by performing two consecutive scans of the femur on each CT scanner. Maximum tension and compression principal strains were computed and compared.

3. Results

The relative difference in dimension at each cross section is presented in Fig. 3. The maximum relative difference in dimensions between all models was less than 2.3%. All QCTFE models had 1,170,000–1,390,000 degrees of freedom and converged to <6.5% relative error in energy norm at $p = 8$. Strains converged to <1% relative error between consecutive solutions (increased polynomial degree). The influence of the geometrical reconstruction, as examined by the FE models with constant $E = 10$ GPa, is presented in Table 3. The maximum RSD in ROIs principal strain that can be attributed to the geometry reconstruction algorithm (segmentation process and pixel size in the various QCT scans in the three considered bones) is 5.5%; however, the average RSD is between 2.1% and 3.1%. Detailed strain values are provided in the Supplemental Material (Appendix B).

Histograms of scans' output data are shown in Fig. 4. Raw HU histograms can be seen in Fig. 4A–C; manipulated raw HU resulting in ash density (ρ_{ash}), which is used to determine inhomogeneous material properties is shown in Fig. 4D–F. Since one proximal femur was cut and cleaned in a previous study, some of the fat and marrow tissue was lost and replaced by air ($HU = -1000$), accounting for the many negative values in the proximal femur's histogram.

The mean and the RSD% of the absolute maximum principal strains at each ROI for all QCTFE models are presented in Fig. 5. These represent all differences in QCTFE models including geometry, material property distribution, and algorithmic influence due to HU manipulation. Maximum RSD in the femur is 7.3%, in the humerus 7.8%, and in the proximal femur 11%; average RSDs are 4.97%, 4.72%, and 6.1%, respectively. Detailed graphs showing the specific values obtained in each FE model are presented in Appendix A. Correlations between each pair of models yielded linear regression equations with slopes varying between 0.93 and 1.05 ($r^2 > 0.96$ for all pairs), the complete linear correlation matrix is provided in Appendix C. ICC estimates and their corresponding 95% CIs are 0.959 [0.901, 0.986], 0.988 [0.971, 0.996], and 0.981 [0.952, 0.995] for the femur, humerus, and proximal femur, respectively.

The location and magnitude of maximum principal strain is the most important information to the medical community because it is associated with risk of fracture. Maximum tensile and compressive principal strains in the femur and proximal femur, and compressive principal strain in the humerus (no tensile significant strains at most loading conditions) are presented in Fig. 6. In the femur, a 6.7% RSD was obtained in the maximum tensile principal strain, with the maximum difference about 10% from the mean value for scanner A. In the humerus, an 8.1% RSD was obtained in the maximum compressive principal strain, with maximum differences for scanners F and G of about –10% and 10% from the mean, respectively. In the proximal femur, a 13.3% RSD was obtained in the maximum compressive principal strain with maximum differences for scanners D and G of about –15% and 15% from the mean value, respectively. The differences in the location of the obtained principal strains compared to the reference point are summarized in Table 4; the maximum difference was <2 mm.

Within-scanner differences in the maximum tensile and compressive principal strains was less than 4.1% for six scanners, but was 7.7% for scanner G. The average difference across all seven scanners was 2.7% (standard deviation 2%).

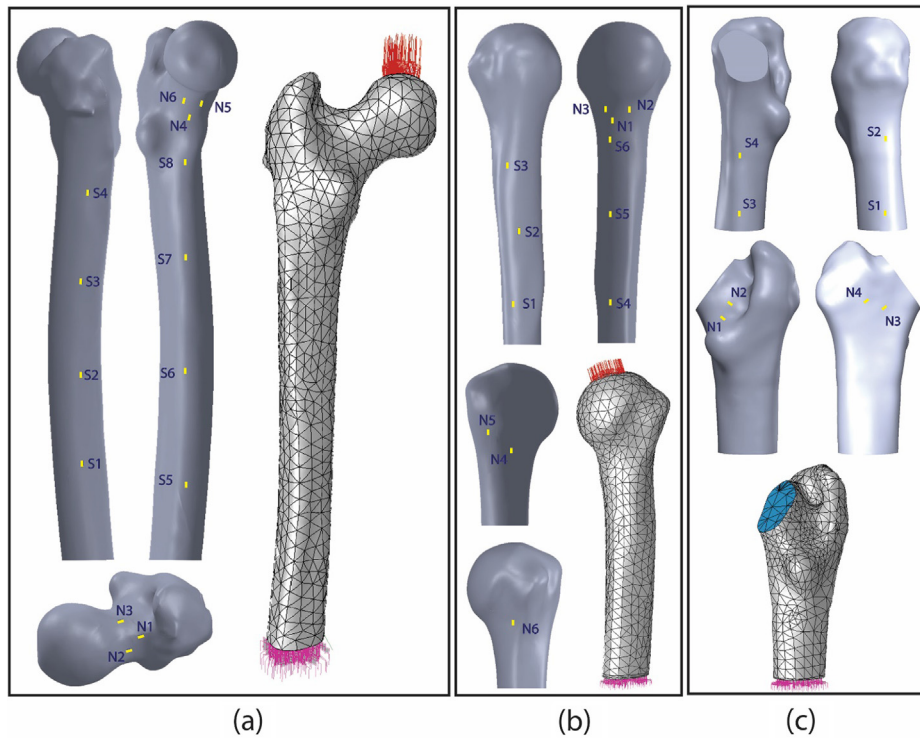


Fig. 2. (a) The femur and regions of interest (ROIs) at which strains were extracted with the QCT-based finite element analysis (CTFEA) model and boundary conditions. (b) The humerus and ROIs with CTFEA model and boundary conditions. (c) The proximal femur with ROIs and CTFEA model with displacement boundary conditions.

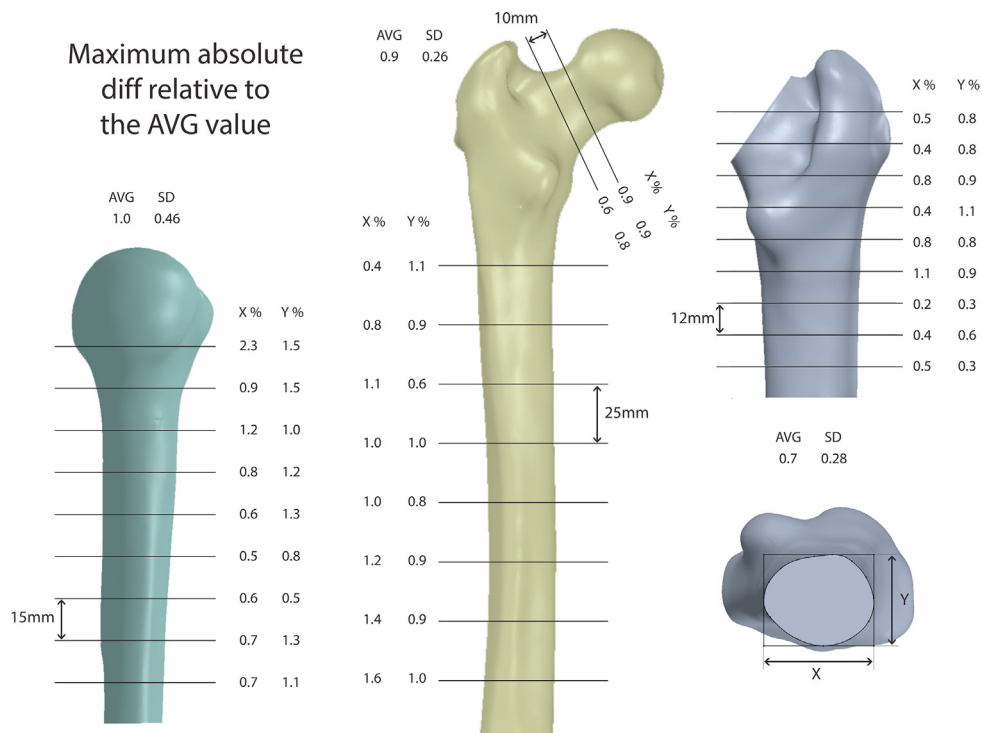


Fig. 3. Maximum difference (relative to scan's average) between all scans at several slice locations along the segmented femurs and humerus. (AVG, average; SD, standard deviation; X, x-axis; Y, y-axis).

4. Discussion

This study investigated whether a rigorous QCT protocol combined with a unique pipeline for the generation of a QCTFE model

enabled reliable values of principal strain in three human bones, regardless of the CT scanner used. Principal strains are quantities used to estimate risk of fracture and indirectly assess bone stiffness, so are of special interest.

Table 3
Mean RSD% and maximum RSD% of ROIs strains for each of the three bones with homogeneous constant Young modulus.

	Femur	Humerus	Femur w/o head
Mean RSD%	2.08%	3.08%	2.51%
Max RSD%	3.45%	5.53%	4.90%
Location of Max RSD	N2	S6	N3

Bone dimensions from the various QCT scans showed very small differences (maximum relative difference < 2.3%). These differences introduced a maximum RSD of 5.5% in the ROIs principal strains for the three bones when homogeneous material properties were used. The average differences were much smaller, usually half of the maximum RSD.

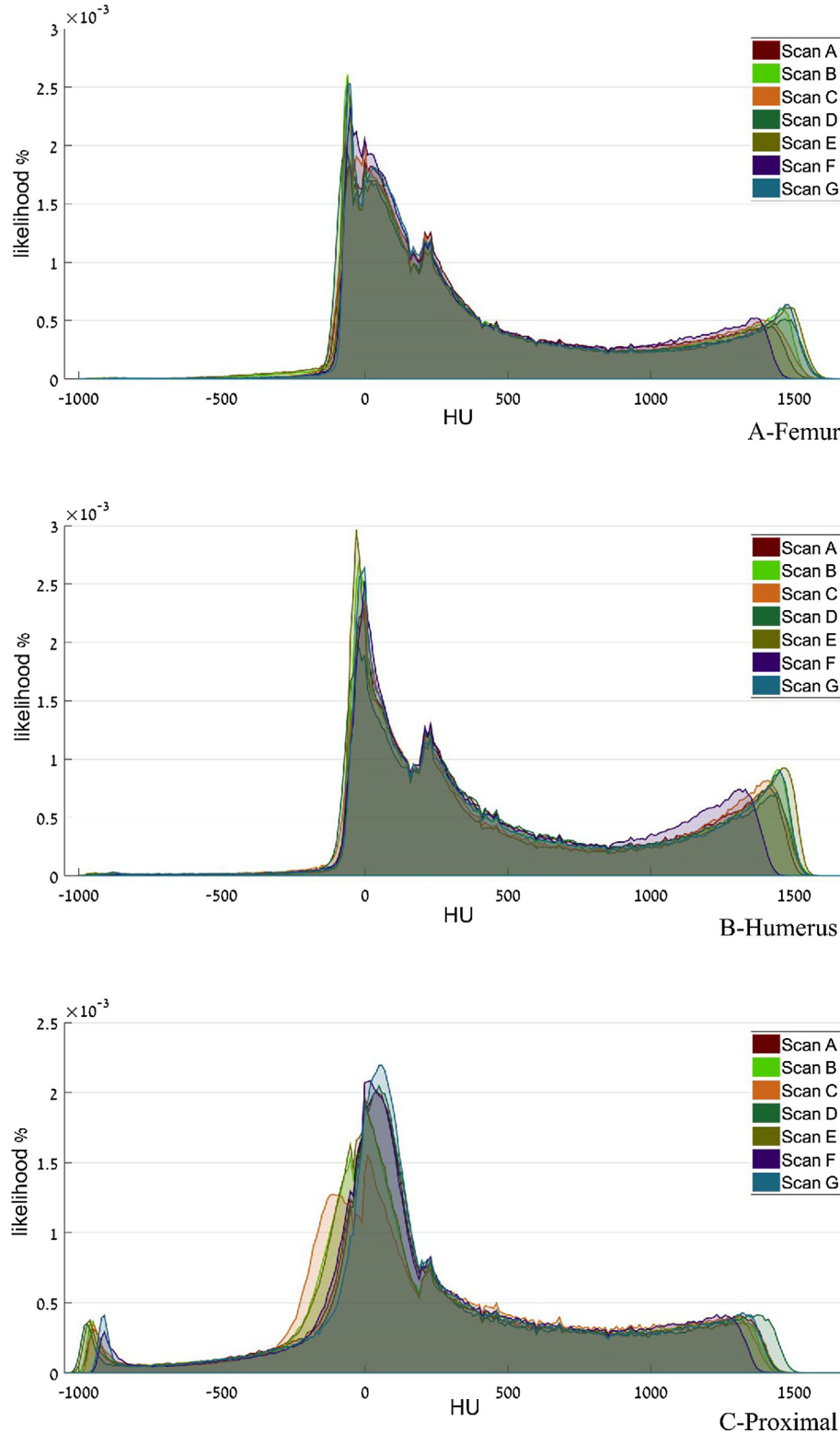


Fig. 4. Histograms of Hounsfield unit (HU) values inside the femur, humerus, and proximal femur in scans A through G. The area under the histogram equals 1. (A–C) Histogram of raw HU values. (D–F) Histogram of ρ_{ash} after phantom calibration, moving average, and boundary corrections.

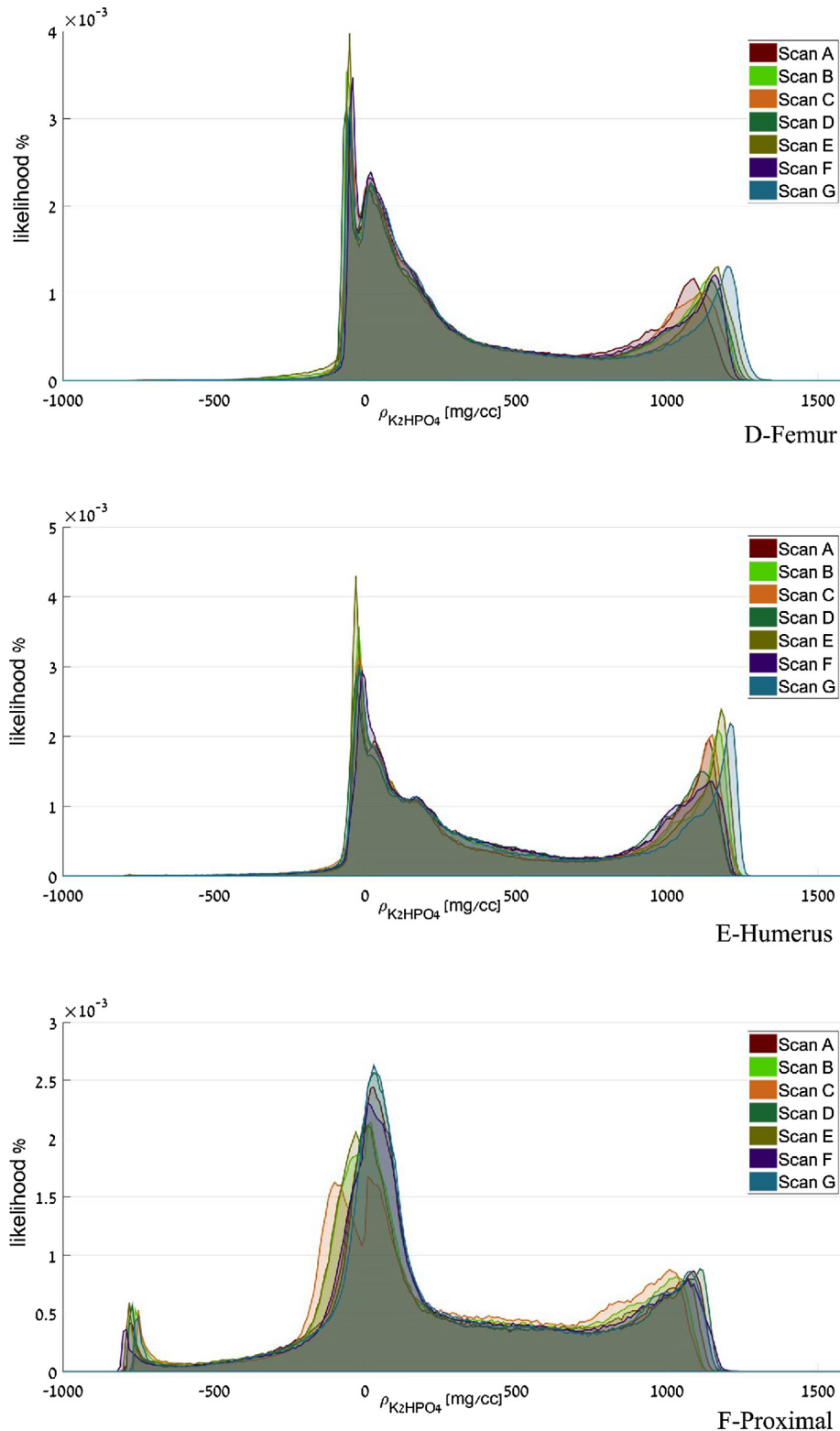


Fig. 4 (continued)

Considering the material properties, the cortex (high HU value) dominates the mechanical behavior of bones. Discrepancy in low HUs has a negligible influence and is deemed unimportant. For example, a tissue having $HU < 200$ ($\rho_{ash} < 0.15$ g/cc), corresponds to $E < 0.5$ GPa, considerably smaller than typical values of $E = 10$ – 20 GPa of the cortex. Focusing on high HU values in the histograms,

discrepancies between raw HU values obtained from the different QCT scans are clearly visible, suggesting that the HU without calibration is scanner-dependent (Fig. 4A–C). Boundary correction and moving average algorithms only influenced the likelihood of HU values already present in the bone (the y axis in the histograms). In contrast, HU values (the x axis) are affected by the phantom

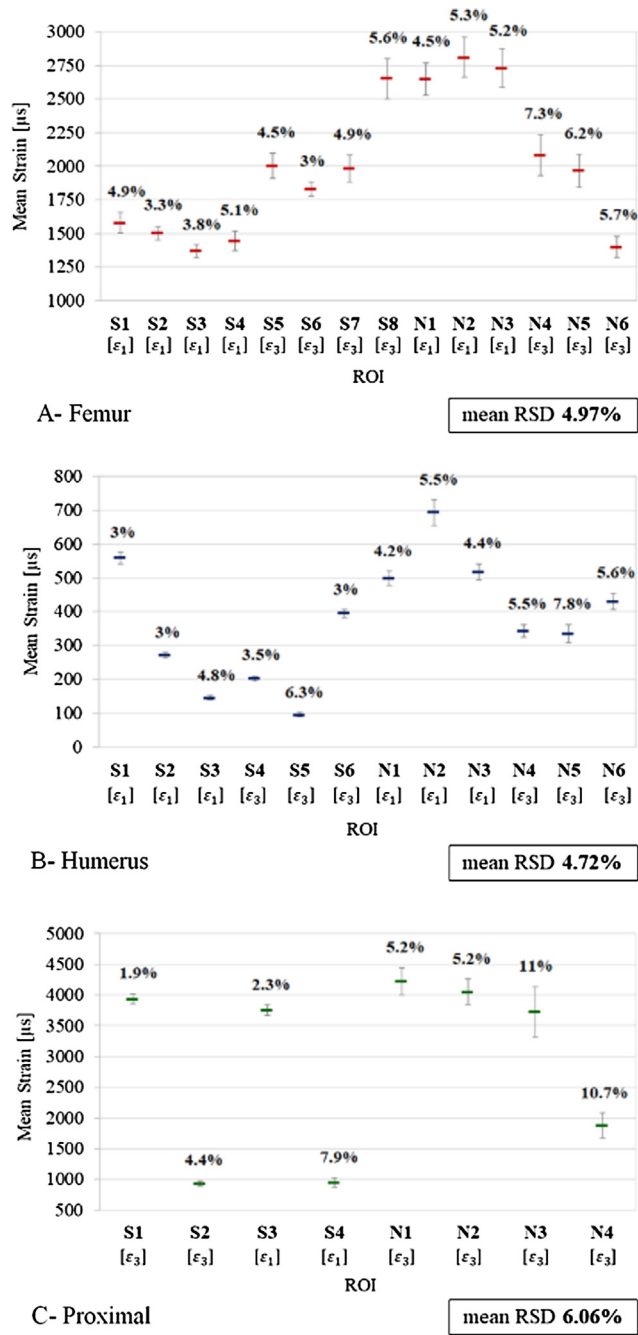


Fig. 5. Mean and RSD values of the maximum absolute principal strains at each ROI across the different scans for the femur (A), humerus (B) and proximal femur (C).

calibration alone; therefore, phantom calibration reduces scanner dependence, although some variation is still present (Fig. 4D–F).

The maximum RSD in the ROIs strains was <8% in the femur and humerus, and <11% in the proximal femur without the head. The mean RSD was about half of the maximum RSD, ≤5% in “regular” bones and <6.1% in the proximal femur. However, the total maximum difference observed between two scanners in all three bones and all ROIs was 20%. Linear correlations between each pair of models showed very good agreement.

ICC values > 0.9 indicate excellent reliability (Koo and Li, 2016) among the different scanners. However, these findings should be interpreted with caution. The ICC highly depends on the variance between the examined subjects, i.e. the ROIs strains. These were

taken from different regions along different bones and thus characterized by high variability. Additionally, the ICC provides only a general measure of the agreement level, with no quantitative estimate of the variability between the scanners.

The maximum tensile/compressive principal strains, the quantities of interest when risk of fracture is considered, were obtained at similar locations in all models (Fig. 6). The high variability in the maximum principal strains values obtained in the proximal femur (RSD < 13.3%) can be related to the highly complex geometry at the unusual location of the maximum strains (Fig. 6C) and thus may not be representative. Using a clinical “soft/body” filter/convolution kernel at 120 kV and calibration with liquid K₂HPO₄ phantoms, the maximum RSD between QCTFE maximum principal strains in “regular” bones (such as the femur and humerus), is <8%. Nonetheless, there may be differences up to 20% between maximum principal strains estimated using two scanners with the most extreme differences; thus, in a longitudinal study only changes larger than 20% in principal strains may be significant. Such analyses are important, for example, to determine prognosis in a patient with osteoporosis or metastases. It is noteworthy that previous experience suggests that in pathological situations such as benign or metastatic tumors, changes in the strain fields for the pathological femur are of tens of percent compared to the healthy femur, so the 20% difference from different scanners would be of smaller significance in these cases (Sternheim et al., 2018).

Repeated scans on same CT systems resulted in an average difference of 2.7% in the maximum principal strains. These findings suggest that one should expect similar or higher variability between CT scanners.

Exposure (mAs) has a negligible influence on differences in QCTFE results between CT systems, as demonstrated in previous studies (Giambini et al., 2015; Nazarian et al., 2008). We conducted two identical scans where a change in the exposure level was the only difference in protocol and obtained almost no change in the HU histograms.

Several previous studies have emphasized the use of phantoms to quantify HU variability between CT scanners. A study by (Suzuki et al., 1991) investigated the variance between QCT scans of cadaveric vertebrae together with K₂HPO₄ phantoms obtained from 16 CT scanners, including 10 different models. They reported “good correlations (r > 0.97) . . . observed for QCT values obtained by various CT scanners.” An excellent review (Cann, 1988) showed good reproducibility of QCT values obtained from several scanners, although CT systems used in the study are by now outdated. These publications however did not evaluate differences in strains computed by QCTFE. To the best of our knowledge, the only study addressing the latter issue examined the femoral fracture load predicted by QCTFE analyses, as assessed with two different CT scanners (Carpenter et al., 2014).

It is important to note that most publications using QCTFE were based on the classical h-version of the FE method, which does not include numerical convergence studies. Numerical errors inherent in h-version techniques may contribute substantially to the differences in predictions. As an example, a difference in strains of ~3% was found at the neck between the FE analysis performed at p = 4 compared to the converged strains at p = 8.

4.1. Limitations and future studies

This study did not consider body size effects that may be taken into consideration using anthropomorphic standardization phantoms (ASPs) to assess inter-scanner differences. Carpenter et al. (2014) found that differences in body size may result in varying estimates of femur strength between scanners. In addition, tube voltage (kV) has an influence on HU distribution histograms. We performed scans using 80–140 kV (data not presented here) and

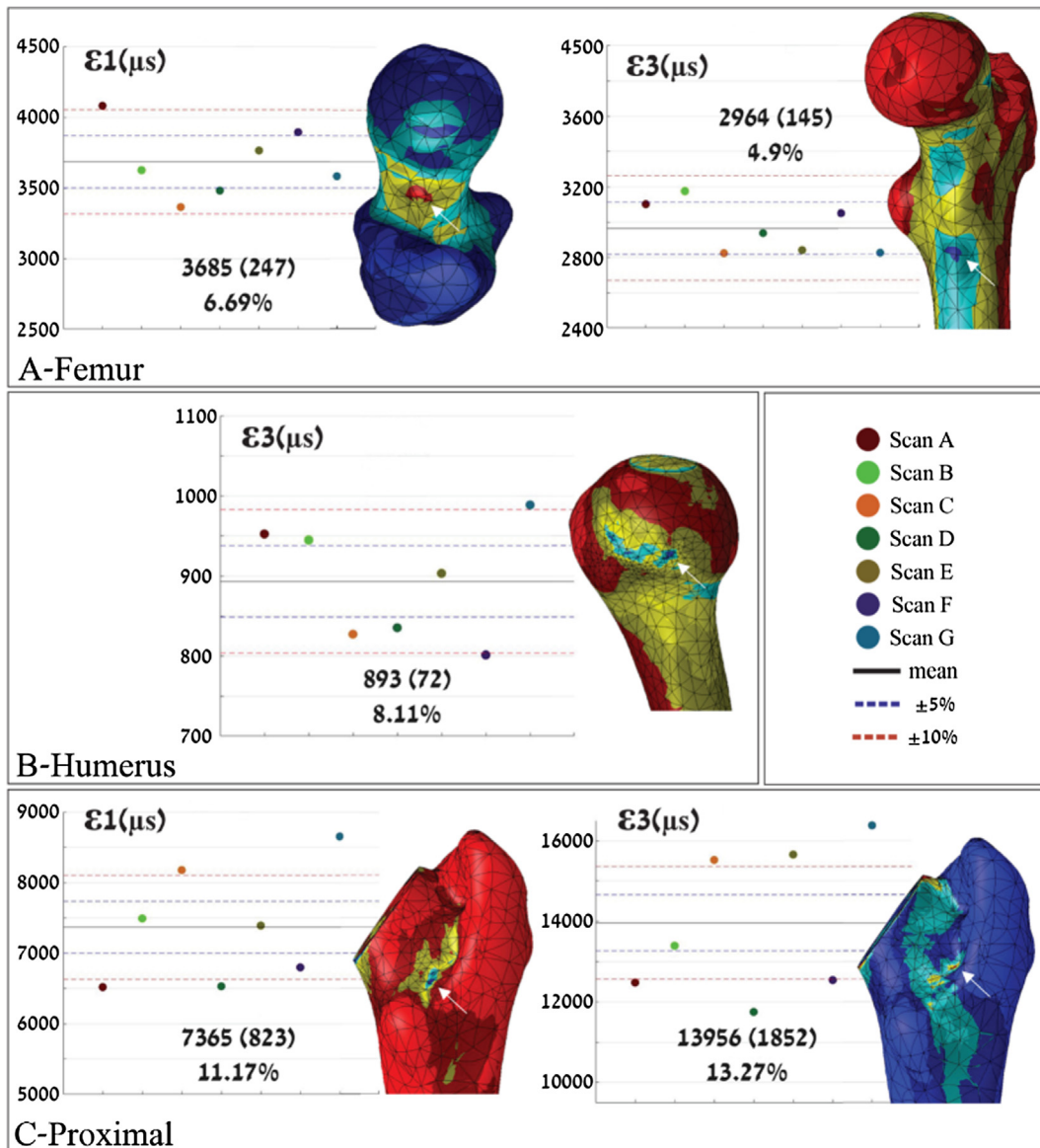


Fig. 6. Maximum tensile/compressive (ϵ_1/ϵ_3) principal strains, in the femur (A), humerus (B), and proximal femur (C). In each panel the mean (SD) and RSD% of the maximal strain is presented. The humerus is under compressive state; thus, no tensile graph is presented.

Table 4

Mean and maximum distances [mm] and standard deviation of the location of the maximum principal strains, relative to the “average location” (QCTFE based on the 7 scanners).

	Femur		Humerus	Proximal Femur	
	ϵ_1	ϵ_3		ϵ_1	ϵ_3
Mean distance [mm]	0.48	0.91	0.66	0.73	1.00
SD [mm]	0.32	0.40	0.23	0.23	0.52
Max distance [mm]	1.10	1.57	1.05	1.01	1.97

will address the influence of kV on estimation of bone’s mechanical response in a future publication.

We studied three manufacturers and four CT scanners at four different medical centers. While these are believed to represent the majority of CT scanners in the Western world, future studies may include a larger number of CT systems and manufacturers.

The conclusions of our study are based only on descriptive statistics. Future studies should include more subjects, i.e. more bones of the same kind.

Finally, although past investigations suggest the use of phantoms in the range of 0–300 mg/cc (Bessho et al., 2007; Miura et al., 2017; Yosibash et al., 2014), cortical tissue has an equivalent mineral density of about 1200 mg/cc, about four times higher. The slope parameter m in Table 2 is sensitive to inaccuracies in the extreme concentration phantoms (0 and 300 mg/cc), thus it strongly influences predicted strains. To improve the calibration, two alternatives will be considered in a future investigation: Using phantom concentrations covering the entire range of HUs, or

preferably, developing phantom-less methods as suggested in (Lee et al., 2017; Suzuki et al., 1991).

4.2. Conclusions

QCTFE analyses of long bones performed by seven different CT scanners showed a maximum 20% differences in principal strains. In a longitudinal study, only changes larger than 20% in principal strains may be significant.

Conflicts of interest

Prof. Yosibash has a financial interest in PerSimiO, a technology company specializing in personalized simulations in orthopedics. Prof. Sosna is a member of the PerSimiO Board of Advisors. Neither Prof. Yosibash or Prof. Sosna derived any direct financial support, research support, or other benefit from the company that could jeopardize their independence in this research. Primary data was jointly controlled by Yekutiel Katz and Gal Dahan. They and the remaining authors have no conflict of interest to declare that could bias the presented work.

Disclosures and acknowledgements

The study was funded in part by a grant from the Milgrom Foundation for Science grant. The authors thank Dr. Gabriel Bartal and Mr. Isaac Yunes at Meir Medical Center, Mr. David Shushan at the Soroka Medical Center, and Mrs. Nathalie Greenberg from the Hadassah-Hebrew University Medical Center for their help and collaboration on the acquisition of the QCT scans. The authors thank Prof. Joyce Keyak from the University of California at Irvine in the USA and Dr. Nir Trabelsi from the Shamon College of Engineering in Israel for interesting discussions. The authors thank Dr. Lena Novack from Ben Gurion University of the Negev and Prof. Malka Gurfine from Tel-Aviv University for their assistance on the statistical analysis and Mrs. Shifra Fraifeld from the Hadassah-Hebrew University Medical Center for helpful editorial assistance.

Appendix A. Supplementary material

Supplementary data to this article can be found online at <https://doi.org/10.1016/j.jbiomech.2019.01.049>.

References

- Bayraktar, H.H., Morgan, E.F., Niebur, G.L., Morris, G.E., Wong, E.K., Keaveny, T.M., 2004. Comparison of the elastic and yield properties of human femoral trabecular and cortical bone tissue. *J. Biomech.* 37, 27–35.
- Bessho, M., Ohnishi, I., Matsuyama, J., Matsumoto, T., Imai, K., Nakamura, K., 2007. Prediction of strength and strain of the proximal femur by a CT-based finite element method. *J. Biomech.* 40, 1745–1753.
- Cann, C.E., 1988. Quantitative CT for determination of bone mineral density: a review. *Radiology* 166, 509–522.
- Carpenter, R.D., Saeed, I., Bonaretti, S., Schreck, C., Keyak, J.H., Streeper, T., Harris, T. B., Lang, T.F., 2014. Inter-scanner differences in *in vivo* QCT measurements of the density and strength of the proximal femur remain after correction with anthropomorphic standardization phantoms. *Med. Eng. Phys.* 36, 1225–1232.
- Dahan, G., Trabelsi, N., Safiran, O., Yosibash, Z., 2016. Verified and validated finite element analyses of humeri. *J. Biomech.* 49, 1094–1102.
- Dall'Ara, E., Luisier, B., Schmidt, R., Kainberger, F., Zysset, P., Pahr, D., 2013. A nonlinear QCT-based finite element model validation study for the human femur tested in two configurations *in vitro*. *Bone* 52, 27–38.
- Dragomir-Daescu, D., Salas, C., Uthamaraj, S., Rossman, T., 2015. Quantitative computed tomography-based finite element analysis predictions of femoral strength and stiffness depend on computed tomography settings. *J. Biomech.* 48, 153–161.
- Enns-Bray, W.S., Ariza, O., Gilchrist, S., Widmer Soyka, R.P., Vogt, P.J., Palsson, H., Boyd, S.K., Guy, P., Crompton, P.A., Ferguson, S.J., Helgason, B., 2016. Morphology based anisotropic finite element models of the proximal femur validated with experimental data. *Med. Eng. Phys.* 38, 1339–1347.
- Giambini, H., Dragomir-Daescu, D., Huddleston, P.M., Camp, J.J., An, K.N., Nassr, A., 2015. The effect of quantitative computed tomography acquisition protocols on bone mineral density estimation. *J. Biomech. Eng.* 137, 114502.
- Goodsitt, M.M., 1992. Conversion relations for quantitative CT bone mineral densities measured with solid and liquid calibration standards. *Bone Mineral* 19, 145–158.
- Hazrati Marangalou, J., Ito, K., van Rietbergen, B., 2012. A new approach to determine the accuracy of morphology-elasticity relationships in continuum FE analyses of human proximal femur. *J. Biomech.* 45, 2884–2892.
- Helgason, B., Gilchrist, S., Ariza, O., Chak, J.D., Zheng, G., Widmer, R.P., Ferguson, S.J., Guy, P., Crompton, P.A., 2014. Development of a balanced experimental-computational approach to understanding the mechanics of proximal femur fractures. *Med. Eng. Phys.* 36, 793–799.
- Katz, Y., Lubovsky, O., Yosibash, Z., 2018. Patient-specific finite element analysis of femurs with cemented hip implants. *Clin. Biomech.* 58, 74–89.
- Keaveny, T.M., Hoffmann, P.F., Singh, M., Palermo, L., Bilezikian, J.P., Greenspan, S.L., Black, D.M., 2008. Femoral bone strength and its relation to cortical and trabecular changes after treatment with PTH, alendronate, and their combination as assessed by finite element analysis of quantitative CT scans. *J. Bone Mineral Res.: Off. J. Am. Soc. Bone Mineral Res.* 23, 1974–1982.
- Keaveny, T.M., Kopperdahl, D.L., Melton 3rd, L.J., Hoffmann, P.F., Amin, S., Riggs, B.L., Khosla, S., 2010. Age-dependence of femoral strength in white women and men. *J. Bone Mineral Res.: Off. J. Am. Soc. Bone Mineral Res.* 25, 994–1001.
- Keller, T.S., 1994. Predicting the compressive mechanical behavior of bone. *J. Biomech.* 27, 1159–1168.
- Keyak, J.H., Lee, I.Y., Skinner, H.B., 1994. Correlations between orthogonal mechanical properties and density of trabecular bone: use of different densitometric measures. *J. Biomed. Mater. Res.* 28, 1329–1336.
- Keyak, J.H., Kaneko, T.S., Tehranzadeh, J., Skinner, H.B., 2005. Predicting proximal femoral strength using structural engineering models. *Clin. Orthop. Relat. Res.*, 219–228.
- Keyak, J.H., Meagher, J.M., Skinner, H.B., Mote Jr., C.D., 1990. Automated three-dimensional finite element modelling of bone: a new method. *J. Biomed. Eng.* 12, 389–397.
- Koo, T.K., Li, M.Y., 2016. A guideline of selecting and reporting intraclass correlation coefficients for reliability research. *J. Chiropract. Med.* 15, 155–163.
- Lee, D.C., Hoffmann, P.F., Kopperdahl, D.L., Keaveny, T.M., 2017. Phantomless calibration of CT scans for measurement of BMD and bone strength-Inter-operator reanalysis precision. *Bone* 103, 325–333.
- McGraw, K.O., Wong, S.P., 1996. Forming inferences about some intraclass correlation coefficients. *Psychol Meth* 1, 30–46.
- Mindways Software, I., 2002. CT calibration phantom user's guide. Mindways Software Inc. Austin, TX, USA.
- Miura, M., Nakamura, J., Matsuura, Y., Wako, Y., Suzuki, T., Hagiwara, S., Orita, S., Inage, K., Kawarai, Y., Sugano, M., Nawata, K., Ohtori, S., 2017. Prediction of fracture load and stiffness of the proximal femur by CT-based specimen specific finite element analysis: cadaveric validation study. *BMC Musculoskelet Disord* 18, 536.
- Nazarian, A., Snyder, B.D., Zurakowski, D., Muller, R., 2008. Quantitative micro-computed tomography: a non-invasive method to assess equivalent bone mineral density. *Bone* 43, 302–311.
- Nishiyama, K.K., Gilchrist, S., Guy, P., Crompton, P., Boyd, S.K., 2013. Proximal femur bone strength estimated by a computationally fast finite element analysis in a sideways fall configuration. *J. Biomech.* 46, 1231–1236.
- Pise, U.V., Bhatt, A.D., Srivastava, R.K., Warkekar, R., 2009. A B-spline based heterogeneous modeling and analysis of proximal femur with graded element. *J. Biomech.* 42, 1981–1988.
- Schileo, E., Balistreri, L., Grassi, L., Cristofolini, L., Taddei, F., 2014. To what extent can linear finite element models of human femora predict failure under stance and fall loading configurations? *J. Biomech.* 47, 3531–3538.
- Schileo, E., Dall'ara, E., Taddei, F., Malandrino, A., Schotkamp, T., Baleani, M., Viceconti, M., 2008a. An accurate estimation of bone density improves the accuracy of subject-specific finite element models. *J. Biomech.* 41, 2483–2491.
- Schileo, E., Taddei, F., Cristofolini, L., Viceconti, M., 2008b. Subject-specific finite element models implementing a maximum principal strain criterion are able to estimate failure risk and fracture location on human femurs tested *in vitro*. *J. Biomech.* 41, 356–367.
- Sternheim, A., Giladi, O., Gortzak, Y., Drexler, M., Salai, M., Trabelski, N., Milgrom, C., Yosibash, Z., 2018. Pathological fracture risk assessment in patients with femoral metastases using CT-based finite element methods. A retrospective clinical study. *Bone* 110, 215–220.
- Suzuki, S., Yamamuro, T., Okumura, H., Yamamoto, I., 1991. Quantitative computed tomography: comparative study using different scanners with two calibration phantoms. *Br. J. Radiol.* 64, 1001–1006.
- Szabó, B., Babúška, I., 1991. Finite element analysis. John Wiley & Sons, New York.
- Trabelsi, N., Yosibash, Z., Wutte, C., Augat, P., Eberle, S., 2011. Patient-specific finite element analysis of the human femur—a double-blinded biomechanical validation. *J. Biomech.* 44, 1666–1672.
- Varga, P., Inzana, J.A., Gueorguiev, B., Sudkamp, N.P., Windolf, M., 2018. Validated computational framework for efficient systematic evaluation of osteoporotic fracture fixation in the proximal humerus. *Med. Eng. Phys.* 57, 29–39.
- Wirtz, D.C., Schiffrers, N., Forst, R., Pandorf, T., Weichert, R., Radermacher, K., 2000. Critical evaluation of known bone material properties to realize anisotropic FE-simulation of the proximal femur. *J. Biomech.* 33, 1325–1330.

- Yosibash, Z., Padan, R., Joskowicz, L., Milgrom, C., 2007a. A CT-based high-order finite element analysis of the human proximal femur compared to in-vitro experiments. *J. Biomech. Eng.* 129, 297–309.
- Yosibash, Z., Plitman Mayo, R., Dahan, G., Trabelsi, N., Amir, G., Milgrom, C., 2014. Predicting the stiffness and strength of human femurs with real metastatic tumors. *Bone* 69, 180–190.
- Yosibash, Z., Tal, D., Trabelsi, N., 2010. Predicting the yield of the proximal femur using high-order finite-element analysis with inhomogeneous orthotropic material properties. *Philos. Trans. Ser. A, Math., Phys., Eng. Sci.* 368, 2707–2723.
- Yosibash, Z., Trabelsi, N., Milgrom, C., 2007b. Reliable simulations of the human proximal femur by high-order finite element analysis validated by experimental observations. *J. Biomech.* 40, 3688–3699.